

Spikes *et al.* (2004), *Annals of Glaciology*, **39**.

## **Variability in Accumulation Rates from GPR Profiling on the West Antarctic Plateau**

Vandy B. Spikes<sup>1,2</sup>, Gordon S. Hamilton<sup>1,2</sup>, Steven A. Arcone<sup>3</sup>, Susan Kaspari<sup>1</sup>, and Paul A. Mayewski<sup>1,2</sup>

University of Maine, <sup>1</sup>Climate Change Institute and the

<sup>2</sup>Department of Earth Sciences, Orono, ME, 04469, USA

<sup>3</sup>U.S. Army ERDC, Cold Regions Research and Engineering Laboratory, Hanover, NH, 03755, USA

### **Abstract**

Isochronal layers in firn detected with ground-penetrating radar (GPR) and dated using results from ice core analyses are used to calculate accumulation rates along a 100-km across-flow profile in West Antarctica. Accumulation rates are shown to be highly variable over short distances. Elevation measurements from global positioning system surveys show that accumulation rates derived from shallow horizons correlate well with surface undulations, which infers that wind redistribution of snow is the leading cause of this variability. Temporal changes in accumulation rate over 25- to 185-year intervals are smoothed to along-track length-scales comparable to surface undulations in order to identify trends in accumulation that are likely related to changes in climate. Results show that accumulation rates along this profile have decreased in recent decades, which is consistent with core-derived time series of annual accumulation rates measured at the two ends of the radar profile. These results suggest that temporal variability observed in accumulation rate records from ice cores and GPR profiles can be obscured by spatial influences, although it is possible to resolve temporal signals if the effects of local topography and ice flow are quantified and removed.

## INTRODUCTION

Snow accumulation rates on the Antarctic ice sheet are known to be highly variable over short distances (e.g. Black and Budd, 1964; Gow and Rowland, 1965; Whillans, 1975, Richardson and others, 1997; Richardson and Holmlund, 1999; Vaughan and others, 1999b) and over short time intervals (e.g. Mosley-Thompson and others, 1995, Kaspari and others, *this volume*). However, accumulation rates in Antarctica are not well characterized, because they have only been assessed using compilations of widely spaced point measurements and low-resolution (~25 km) passive microwave data (e.g. Vaughan and others, 1999a; Giovinetto and Zwally, 2000), which do not capture the full range of accumulation variability, and may not produce an accurate spatial mean (e.g. Richardson and others, 1997; Richardson and Holmlund, 1999). This observation has important implications for studies of ice sheet mass balance and sea level rise, because accumulation of snow is a key quantity for mass balance calculations (e.g. Shabtaie and Bentley, 1987; Hamilton and others, 1998; Wingham and others, 1998; Joughin and Tulaczyk, 2002; Rignot and Thomas, 2002).

The objectives of this study are to develop a better understanding of the spatial distribution of snow accumulation on the West Antarctic plateau, to investigate how topography and ice flow influence measurements of accumulation rate, and to examine the spatial persistence of temporal variations observed in accumulation records. To address these issues, accumulation rates are derived from ground-penetrating radar (GPR) profiling of firn stratigraphy (Arcone and others, *this volume*) and dated ice cores (Dixon and others, *this volume*). The results are interpreted using elevation data from global positioning system (GPS) surveys (Hamilton and Spikes, 2003). We demonstrate that the

continuous reflections identified in this particular 400 MHz radar profile have an isochronal accuracy of <1 year when dated and traced between ice core sites. This result justifies the use of these horizons for determining the spatial distribution of historical accumulation rates.

## STUDY AREA

The data described here were collected in December 2000 along a 100-km transect across the West Antarctic ice sheet (WAIS) and represent a small portion of the data collected during the United States component of the International Trans Antarctic Scientific Expedition (US ITASE) (Fig. 1). The GPR and GPS data were collected while traveling (azimuth of 290°) between two ice core sites, 00-4 to 00-5 (Fig. 1b). This transect is located more than 400 km from open water and is situated near the ice divide that separates the Ross and Amundsen sea drainage basins. Based on elevation contours from a digital elevation model (Liu and others, 1999), ice flows across this transect at an azimuth of ~180°, which is nearly perpendicular (~20° from normal) to the orientation of the profile (Fig. 1b). Estimated ice thickness in this region exceeds 2000 m (Lythe and others, 2000). According to Tzeno and others (1993), the winds in this region are katabatic, or gravity driven, and are therefore approximately parallel to the direction of ice flow. The net elevation difference between 00-4 and 00-5 is 140 m. A discussion of the source for and mechanisms of precipitation in this region is presented in a related article by Kaspari and others (*this volume*).

## SIMPLIFYING THE RADAR PULSE

A 400 MHz short-pulse radar system that radiates a 1.5-cycle pulse (Fig. 2a) lasting about 3.8 ns was used to examine the internal stratigraphy along US ITASE traverses. The vertical resolution is approximately 35 cm in firn, and the system can track stratigraphy to depths of ~100 m (Arcone and others, *this volume*). In firn of dielectric constant  $\epsilon = 2.4$  (typical value for dry polar snow) this pulse duration provides a layer interface separation resolution of approximately 35 cm. This spacing is generally greater than the separation of annual layers at depth in polar firn. The radar profile discussed here reveals numerous events represented by pulse shapes similar to that in Figure 2a, which are most likely responses to one or more closely-spaced thin layers spanning a thickness of 10 cm or less. To simplify the appearance of the profile horizons, we deconvolved (spiked) the profile and applied a Hilbert magnitude transform, as shown in Figure 2a. The consistency of the phase structure of this pulse shape throughout the profile in Figure 2b provides the basis for our confidence that we have tracked the leading edge of an isochronal event or series of events.

## DEFINING THE DEPTH-AGE RELATIONSHIP

To determine the relationship between depth and age for the upper ~60 m of firn at each end of the radar profile, ice cores collected at 00-4 and 00-5 were analyzed for soluble major ion content (e.g. Dixon and others, *this volume*) and density. High resolution chemical analysis (30–50 measurements per meter) was used to define each core-chemistry year on the basis of a winter-spring peak in  $\text{Na}^+$ ,  $\text{Cl}^-$ ,  $\text{Ca}^+$ ,  $\text{Mg}^{2+}$ , and  $\text{K}^+$  combined with spring-summer peaks in both  $\text{NO}_3^-$  and excess non-sea salt (nss)  $\text{SO}_4^{2-}$

(Whitlow and others, 1992; Legrand and Mayewski, 1997). Extreme events, such as the 1815 A.D. Tambora volcanic eruption provide absolute age horizons within each core that are easily identified in  $\text{nssSO}_4^{2-}$  profiles (Fig. 1c). The dimensions and mass of individual core sections (average length is  $\sim 1$  m) were measured to develop a density profile for each site (Fig. 1c). The round-trip travel time of each returned radar pulse (maximum of 741 ns) was converted to depth using the density profiles and the well-known relationship between firn density and dielectric constant (Kovacs and others, 1995) which determines the radio wave velocity (e.g. Richardson and Holmlund, 1999). These procedures allow us to plot the depth and age of each ice core sample against its corresponding radar horizon (e.g. Fig. 2b).

#### TESTS OF ISOCHRONAL ACCURACY

We tested the five darkened horizons in Figure 2b for isochronal accuracy by tracking their leading edge from one dated core to the other. The maximum age difference found for all the horizons tested is  $< 1$  year, including the deepest horizon that dates to 1815 A.D. This high degree of isochronal accuracy suggests that there is little or no error induced by layer variations, which we attribute to our trace acquisition rate ( $\sim 1$  trace/15 m), traverse speed ( $\sim 3$  m/s), and stacking rate during acquisition. Each of the 6641 traces in our final profile represents a stack of approximately 150 traces so that layer variations are well averaged.

It is unlikely that our procedure for depth calibration introduces any significant error, despite the 1-m core lengths used for density calculations. For example, if the average density of a 1-m core section is  $600 \text{ kg m}^{-3}$ , the round-trip delay of the radar

signal is 10.051 ns. Assuming an exaggerated inhomogeneity of  $550 \text{ kg m}^{-3}$  for the top half and  $650 \text{ kg m}^{-3}$  for the bottom half of the core, the error in time delay through each meter of core is only -0.002 ns. The cumulative error at 60 m depth would be 0.12 ns (~1 cm) within the >600 ns record. In addition, we assume that the top two meters are at the same density as the third meter ( $\sim 400 \text{ kg m}^{-3}$ ) because our density profiles generally begin at a depth of 2 m. An actual density of  $300 \text{ kg m}^{-3}$  for the top two meters would give a time delay error of 1.1 ns (~10 cm), which corresponds to less than one year at a depth of 50 m.

A more likely source of error is related to difficulties in tracking some of the deeper layers where undulations on the ice sheet surface are more pronounced. The continuity of the horizons is most evident within 60 km of site 00-4 (Fig. 2b), where the ice sheet surface is relatively smooth (Fig. 3, *top right*). Beyond 60 km, surface undulations affect the local accumulation rate, as noted in previous studies (Black and Budd, 1964; Gow and Rowland, 1965; Whillans, 1975; Mosley-Thompson and others, 1995; Venteris and Whillans, 1998; Vaughan and others, 1999b). The folded appearance of the radar horizons indicates that more snow accumulates in depressions than on hills. As the apparent folding becomes amplified with depth, the incidence angle (stratigraphic dip) between radar pulses and stratigraphic layers increases. An incidence angle of only 0.4 degrees, which is typical for this profile, provides a round-trip phase delay of almost half a wavelength between consecutively recorded traces. Therefore, this delay reduces return strengths by causing destructive interference and may affect our ability to track an individual horizon. Given this effect, the discernable leading edges that we tracked may represent one of a few closely spaced historical events.

## DETERMINING SNOW ACCUMULATION RATES

To determine historical accumulation rates at any point along the profile, the position and density profile of each trace was first estimated. We digitized each of the darkened radar horizons in Figure 2b according to trace number (1-6641) and round-trip travel time (0-741 ns). Each trace was post-processed for position and elevation using simultaneously recorded GPS data (Hamilton and Spikes, 2003) that were recorded as the expedition moved across the ice sheet at  $\sim 3 \text{ m s}^{-1}$ . Maximum uncertainties in the GPS positions never exceed 0.2 m (Hamilton and Spikes, 2003). Based on the time when GPR data collection began (obtained from the kinematic GPS receiver) and the trace acquisition rate, we estimate the time when each trace was acquired then interpolate the GPS data to each of these times. Density profiles for all 6641 traces between the two core sites were estimated using linear interpolation.

Accumulation rates,  $\dot{b}$ , for each trace were calculated as follows. The interpolated density profiles and round-trip travel times were used to calculate the water equivalent (w.e.) depth to each horizon, which is divided by the age of the horizon to yield the time-averaged accumulation rate,  $\bar{b}$ , since that layer was deposited. This calculation was performed for all 6641 traces that make up each of the five horizons (Fig. 2b) to produce the along-track accumulation rate,  $\bar{b}_r$ , for each horizon at each trace (subscript r). A long-term  $\bar{b}_r$  is calculated using the deepest digitized horizon, which corresponds to an age of 1815 A.D. The same calculation scheme is used to calculate  $\bar{b}_r$  for the intervals between consecutive horizons.

The uncertainties associated with each calculated  $\bar{b}_r$  vary with depth. Estimated uncertainties are based on three components: layer thinning due to ice advection (0 at surface, 1 cm at 60 m firm depth), the cumulative uncertainty introduced by our procedure for depth calibration (10 cm at 2 m firm depth, 11 cm at 60 m firm depth), and the isochronal accuracy of each horizon (1 year for all depths). All possible combinations of these uncertainties were used in sensitivity tests to determine how calculated accumulation rates vary with depth. Results indicate that uncertainties at a firm depth of 10 m are ~3.8% of the calculated  $\bar{b}_r$ . The uncertainties decrease to ~0.5% of  $\bar{b}_r$  at a firm depth of 60 m. Spatially averaging the calculated  $\bar{b}_r$  further reduces the associated uncertainties.

## RESULTS

Accumulation rates derived from each of the digitized horizons (Fig. 2b) are presented in Figure 3 (*center right*). The maximum spatial variability of long-term  $\bar{b}_r$  along this 100-km transect is 32% (std. dev. = 18%), when comparing the range of  $\bar{b}_r$  (0.098 to 0.195 m a<sup>-1</sup> w.e.) to the profile average of 0.144 m a<sup>-1</sup> w.e. (Fig. 3, *center right*). The standard deviation of  $\bar{b}_r$  from the linear fit in Figure 3 (*center right*) is 9%. The radar-derived accumulation rates agree perfectly with the core-derived accumulation rates at core sites 00-4 (0.192 m a<sup>-1</sup> w.e.) and 00-5 (0.145 m a<sup>-1</sup> w.e.), because the ice cores are used to calibrate the radar technique. However, the average accumulation rate of 0.169 m a<sup>-1</sup> w.e., based on the two ice cores, is 17% higher than the radar-derived average for the 100-km transect. These results are consistent with Richardson and others (1997) and

Richardson and Holmlund (1999), who indicate that widely spaced point measurements do not capture the wide range of spatial variability in accumulation rate, nor do they produce an accurate spatial mean.

## DISCUSSION

### Topographic Influence

The largest component of the spatial variability in  $\bar{b}_r$  (Fig. 3, *center right*) appears to be related to ice sheet surface topography. The large-scale trend of decreasing  $\bar{b}_r$  (linear fit =  $-0.07 \text{ cm a}^{-1} \text{ km}^{-1}$ ) may be an orographic effect due to the steady 140 m rise in elevation from 00-4 to 00-5 (linear fit =  $1.4 \text{ m km}^{-1}$ ) (Fig. 3), but it could also be related to geographic differences between the two sites. For example, 00-4 is located on a relatively flat portion of the ice sheet that is within 20 km of an ice divide, and 00-5 is situated on the leeward flank of an ice ridge that could partially block the supply of moisture from the ocean. Superimposed on the regional trend are local variations in accumulation rate that are related to surface undulations (e.g. Black and Budd, 1964; Gow and Rowland, 1965; Whillans, 1975, Richardson and others, 1997; Richardson and Holmlund, 1999; Vaughan and others, 1999b), which is supported by the observation that local accumulation rates are highest in basins and lowest on peaks (Fig. 3, *top and center right*).

In Figure 3 (*bottom right*), the gradients along the  $\bar{b}_r$  curve,  $k_b$ , indicate that accumulation varies by up to  $3 \text{ cm a}^{-1} \text{ km}^{-1}$  (std. dev. =  $0.55 \text{ cm a}^{-1} \text{ km}^{-1}$ ) while gradients along the elevation curve,  $k_{el}$ , have a maximum of  $11 \text{ m km}^{-1}$  (std. dev. =  $2 \text{ m km}^{-1}$ ). These gradients were calculated according to changes in each variable measured over a

distance of ~150 m ( $\pm 5$  traces). Both  $k_b$  and  $k_{el}$  are presented as absolute values in Figure 3 (*bottom right*) to demonstrate the strong correlation between these two variables. The sign of the correlation coefficients in Table 1 show that  $\bar{b}_r$  and surface undulations are out of phase when both positive and negative gradients are considered. The  $k_b$  curve based on the most recent interval (1966-2000) is presented in Figure 3 (*bottom right*), because it has the best correlation with  $k_{el}$  (Table 1).

The strength of the correlations in Table 1 could depend upon the orientation of the radar profile with regard to dominant wind direction. For example, Black and Budd (1964) suggest that the highest  $\bar{b}$  should occur on the windward flanks of surface undulations, but their study was approximately parallel with the dominant wind direction. In contrast, our profile is nearly perpendicular to the dominant wind direction, and we observe the highest  $\bar{b}$  near the middle of basins (e.g. Whillans, 1975). However, the orientation of the profile does not explain the reduction in correlation between  $k_b$  and  $k_{el}$  with increasing interval age (Table 1), which is likely related to ice advection, because the older layers were deposited farther up-glacier of the radar transect where the topographic influences are presumably different.

### Resolving Climatic Influence

The  $\bar{b}$  data in Figure 4 reveal that the largest amount of variability is observed on annual time-scales. Because  $\bar{b}$  in this region are less than the vertical resolution of our radar system, annual variability must be addressed using the high-resolution ice cores (e.g. Kaspari and others, *this volume*). The annual  $\bar{b}$  at core sites ranges from 5% to 65%

(std. dev. = 22%) when calculated as the percent difference from each core-derived average (Fig. 4, *left*). This high degree of variability is regarded as significant because it often exceeds 16%, which is the estimated uncertainty introduced by sastrugi (Whillans, 1978; Venteris and Whillans, 1998). Longer-term trends (on the order of decades to centuries) in the annual  $\bar{b}$  records related to topography and ice advection have also been considered (Kaspari and others, *this volume*). These high-resolution records show that annual snowfall rates in this region have decreased since 1970.

Accumulation variability on multi-decadal time-scales (25 to 48 years) is determined for intervals between consecutive radar horizons (Fig. 4, *top right*). Standard deviations for each of these intervals vary between 14.1 and 21.1% (Table 2), and the maximum deviation is 29% (Figure 4, *center right*). Percent changes in accumulation rate for each point along-track are determined using the long-term  $\bar{b}_r$  (1815-2000) as a reference interval (Fig. 4, *center right*). Much of the variability in Figure 4 (*center right*) is related to surface undulations and ice flow, which complicates the search for climate signals within each accumulation record.

A clearer picture of changes related to climate emerges when the short-scale spatial variations are smoothed to length-scales that are comparable to surface undulations, which are generally less than 10 km. Using a 10-km running average, multi-decadal variability identified near 00-4 is found to be consistent over distances of ~50 km (Fig 4, *bottom right*). The smoothed profiles also suggest that a less stable climatic regime operates beyond the 50-km mark (Fig 4, *bottom right*), although a portion of the remaining variability may be related to larger-scale topographic, orographic, and geographic effects.

Further isolation of a climate signal may be achieved by calculating the mean  $\bar{b}_r$  for each interval, which also reduces the uncertainties to  $<2 \text{ mm a}^{-1}$  w.e. for all intervals (Table 2). Table 2 shows that typical changes between the means of adjacent intervals are on the order of  $\sim 5\%$  ( $\sim 0.007 \text{ m a}^{-1}$  w.e.) of the regional mean. The largest increase was  $9.9\%$  ( $\sim 0.014 \text{ m a}^{-1}$  w.e.) of the regional mean, which occurred between the 1848-1893 (45-years) and 1893-1941 (48-years) intervals. The largest decrease was  $7.8\%$  ( $\sim 0.011 \text{ m a}^{-1}$  w.e.) of the regional mean, which occurred between the 1941-1966 (25-years) and 1966-2000 (34-years) intervals. This result is consistent with results from the analyses of annual accumulation records (Kaspari and others, *this volume*), which show that this region has experienced a 2 – 9% (00-4 and 00-5, respectively) decrease in accumulation rate since 1970.

## CONCLUSIONS

Continuous radar profiling along a 100-km transect reveals that accumulation rates on the West Antarctic plateau can vary by up to  $3 \text{ cm a}^{-1}$  over a distance of 1 km, although they typically vary at a rate of  $0.55 \text{ cm a}^{-1} \text{ km}^{-1}$ . Wind redistribution of snow around surface undulations is the leading cause of this variability, which is consistent with other studies (e.g. Black and Budd, 1964; Gow and Rowland, 1965; Whillans, 1975; Richardson and others, 1997; Richardson and Holmlund, 1999; Vaughan and others, 1999b). Further characterization of the spatial distribution of snow accumulation on the Antarctic plateau will require additional continuous measurements of the kind presented here.

The advection of ice through surface undulations is found to have an impact on estimates of accumulation rate, which suggests that temporal variability observed in accumulation rate records from ice cores and GPR profiles can be obscured by spatial influences. However, it is possible to resolve temporal signals if the effects of local topography and ice flow are considered. An apparent climate signal identified here is that accumulation rates along this portion of the West Antarctic plateau have decreased in recent decades, which agrees with results from ice core analyses in this region (Kaspari and others, *this volume*).

### **Acknowledgements**

Funding for this research was provided through a grant from the National Science Foundation (OPP-0196441) to GSH and a National Aeronautics and Space Administration Earth System Science Fellowship (NGT5-30426) to VBS. We would like to thank Olaf Eisen, Massimo Frezzotti, and an anonymous reviewer for their helpful comments.

### **References**

- Arcone, S.A., V.B. Spikes, G.S. Hamilton and P.A. Mayewski. 2003. Stratigraphic continuity in 400-MHz short-pulse radar profiles of firn in West Antarctica. *Ann. Glaciol.*, **39**-this volume.
- Black, H.P. and W. Budd. 1964. Accumulation in the region of Wilkes Land, Antarctica. *J. Glaciol.*, **5**, 3-15.
- Dixon, D.A., P.A. Mayewski, S. Kaspari, S. Sneed and M. Handley. 2003. 200-year sub-annual record of sulfate in West Antarctica, from 16 ice cores. *Ann. Glaciol.*, **39**-this volume.
- Giovinetto, M. and J. Zwally. 2000. Spatial distribution of net surface accumulation on the Antarctic ice sheet, *Ann. Glaciol.*, **31**, 171–178.
- Gow, A.J. and R. Rowland. 1965. On the relationship of snow accumulation to surface topography at “Byrd Station,” Antarctica. *J. Glaciol.*, **5**(42), 843–847.

- Hamilton, G.S., I. Whillans and P. Morgan. 1998. First point measurements of ice sheet thickness changes in Antarctica. *Ann. Glaciol.*, **27**, 125-129.
- Hamilton, G.S. and V.B. Spikes. 2003. Assessing the performance of a digital elevation model of Antarctica using precision kinematic GPS profiling, *Global and Planetary Change*, in press.
- Joughin, I. and S. Tulaczyk. 2002. Positive mass balance of the Ross Ice Streams. *Science*, **295**, 476-480.
- Kaspari, S., P.A. Mayewski, D.A. Dixon, V.B. Spikes, S.B. Sneed, M.J. Handley and G.S. Hamilton. 2003. Climate variability in West Antarctica derived from annual accumulation rate records from ITASE firn/ice cores. *Ann. Glaciol.*, **39**-this volume.
- Kovacs A., A.J. Gow and R. Morey. 1995. A reassessment of the in-situ dielectric constant of polar firn, CRREL Report 93-26, 22 pages, U. S. Army ERDC Cold Regions Research and Engineering Laboratory, Hanover, NH.
- Legrand, M. and P.A. Mayewski. 1997. Glaciochemistry of polar ice cores: A review. *Rev. Geophys.*, **35**, 219–1243.
- Liu, H., K. Jezek and B. Li. 1999. Development of an Antarctic digital elevation model by integrating cartographic and remotely sensed data: A geographic information system based approach. *J. Geophys. Res.* **104**(10), 23199-23213.
- Lythe, M.B., D.G. Vaughan and the BEDMAP Consortium. 2000. BEDMAP - bed topography of the Antarctic. 1:10,000,000 scale map. BAS (Misc) 9. Cambridge, British Antarctic Survey.
- Mosley-Thompson, E., L. G. Thompson, J. F. Paskievitch, M. Pourchet, A. J. Gow, M. E. Davis and J. Kleinman. 1995. Recent increase in south pole snow accumulation. *Ann. Glaciol.*, **21**, 131–138
- Rignot, E. and R.H. Thomas. 2002. Mass balance of polar ice sheets. *Science*, **297**, 1502-1506.
- Richardson, C., E. Aarholt, S.E. Hamran, P. Holmlund and E. Isaksson. 1997. Spatial distribution of snow in western Dronning Maud Land, East Antarctica, mapped by a ground-based snow radar. *J. Geophys. Res.*, **102**(B9), 20343-20353.
- Richardson, C. and P. Holmlund. 1999. Spatial variability at shallow snow-layer depths in central Dronning Maud Land, East Antarctica. *Ann. Glaciol.*, **29**, 10-16.
- Shabtaie, S. and C. Bentley. 1987. West Antarctic ice streams draining into the Ross Ice Shelf: configuration and mass balance. *J. Geophys. Res.*, **92**(2), 1311-1336.
- Tzengo, R., D.H. Bromwich and T.R. Parish. 1993. Present-day Antarctic climatology of the NCAR community climate model version 1. *J. Clim.*, **6**(2), 205-226.
- Vaughan, D.G., J.L. Bamber, M. Giovinetto, J. Russell and A.P. Cooper. 1999a. Reassessment of net surface mass balance in Antarctica, *J. Clim.*, **12**, 933–946.
- Vaughan D.G., H.F. Corr, C.S. Doake and E.D. Waddington. 1999b. Distortion of isochronous layers in ice revealed by ground-penetrating radar. *Nature*, **398**, 323-326.

- Venteris, E. and I. Whillans. 1998. Variability of accumulation rate in the catchments of Ice Streams B, C, D, and E, Antarctica. *Ann. Glaciol.*, **27**, 227-230.
- Whillans, I.M. 1975. Effect of inversion winds on topographic detail and mass balance on inland ice sheets. *J. Glaciol.*, **14**(70), 85-90.
- Whillans, I.M. 1978. Surface mass-balance variability near Byrd Station, Antarctica, and its importance to ice core stratigraphy. *J. Glaciol.*, **20**(83), 301-310.
- Whitlow, S., P.A. Mayewski and J.E. Dibb. 1992. A comparison of major chemical species input timing and accumulation at South Pole and Summit Greenland. *Atm. Env.*, **26A**, 2045–2054.
- Wingham, D.J., A.J. Ridout, R. Scharro, R.J. Arthern and C.K. Shum. 1998. Antarctic elevation change from 1992 to 1996. *Science*, **282**, 456-458.

**Tables and figures with captions.**

<i>Interval (Years A.D.)</i>	<i>Correlation coefficient</i>
1815-2000	-0.39
1848-2000	-0.47
1893-2000	-0.49
1941-2000	-0.51
1966-2000	-0.50
1941-1966	-0.42
1893-1941	-0.36
1848-1893	-0.32
1815-1848	-0.26

*Table 1:* Correlation between along-track gradients in  $\bar{b}_r$  and surface slope (Fig. 3, *bottom right*). Negative correlations indicate that large  $\bar{b}_r$  are typically associated with topographic depressions and small  $\bar{b}_r$  are associated with crests/flanks. The correlations are best for the youngest strata, because these have been least affected by advection through a series of undulations.

<i>Interval (Years A.D.)</i>	<i>Avg. accumulation rate (m a<sup>-1</sup> w.e.)</i>	<i>Percent difference (%)</i>	<i>Standard deviation (%)</i>
1966-2000	0.141 ± 0.0016	-2.2 ± 1.2	15.6
1941-1966	0.151 ± 0.0008	5.1 ± 0.6	19.1
1893-1941	0.151 ± 0.0004	5.1 ± 0.34	14.1
1848-1893	0.137 ± 0.0003	-4.8 ± 0.2	16.8
1815-1848	0.142 ± 0.0002	-1.7 ± 0.16	21.1

*Table 2.* Multi-decadal  $\bar{b}_r$  expressed as the 100-km mean for each interval, the percent difference between the interval mean and the long-term regional mean (0.144 m a<sup>-1</sup>). Each of these means comprises 6641 measurements, which greatly reduces the 2s uncertainties. The final column is the standard deviation of  $\bar{b}_r$  for each interval, which is calculated relative to the long-term regional mean.

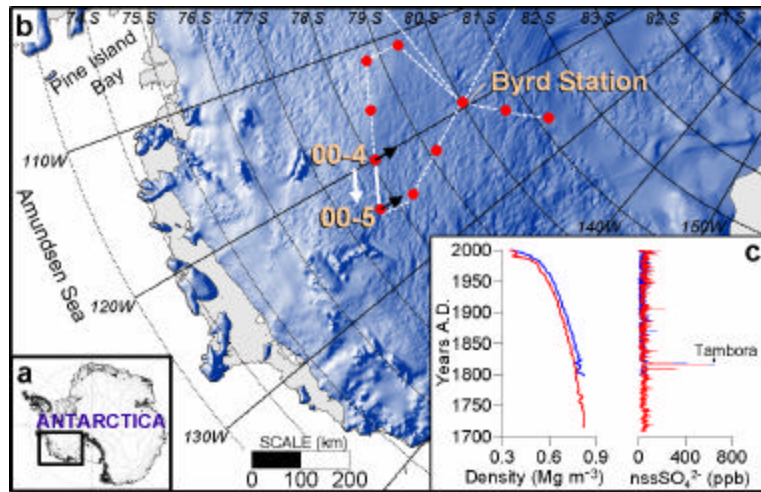


Figure 1. Location maps and ice core data. a) Continent-scale map of Antarctica. b) Portion of West Antarctica (boxed region in a) showing some of the US ITASE traverse routes (white lines). Red circles indicate where ice cores were collected. The solid white line represents the transect along which the radar profile was collected between 00-4 and 00-5. The white arrow indicates the direction of travel during data acquisition. The shaded relief map was generated from a digital elevation model (Liu and others, 1999), which was also used to estimate ice flow directions at 00-4 and 00-5 (black arrows). c) Ice core density and chemistry ( $\text{nssSO}_4^{2-}$ ) profiles for 00-4 (blue) and 00-5 (red).

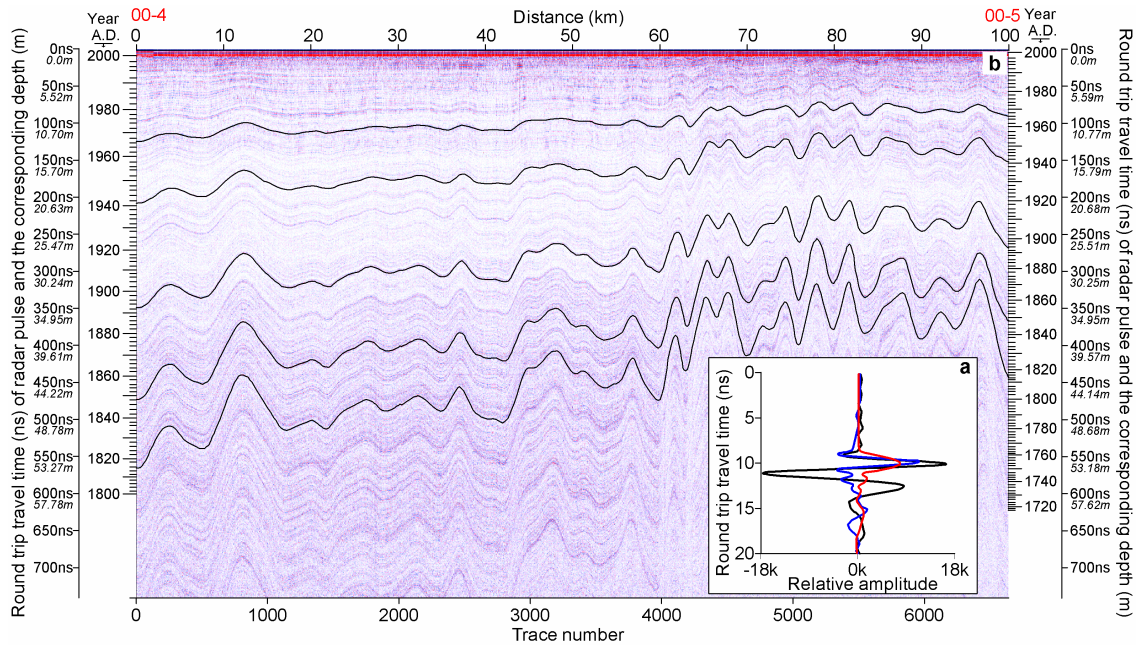


Figure 2. Radar data collected between US ITASE sites 00-4 and 00-5. a) 400-MHz pulse shape as reflected by a high-density layer in firn (black line). The pulse was deconvolved with a spiking routine (blue line) before performing the Hilbert magnitude transform (red line). b) Radar profile after deconvolution and Hilbert magnitude transformation. The darkened horizons are tracked (black lines) to illustrate isochronal continuity between core sites. The deepest visible horizon at Site 4 has been tracked the entire distance (~550 km along-track) to Byrd Station. Signal fading related to surface undulations is apparent beyond 60 km.

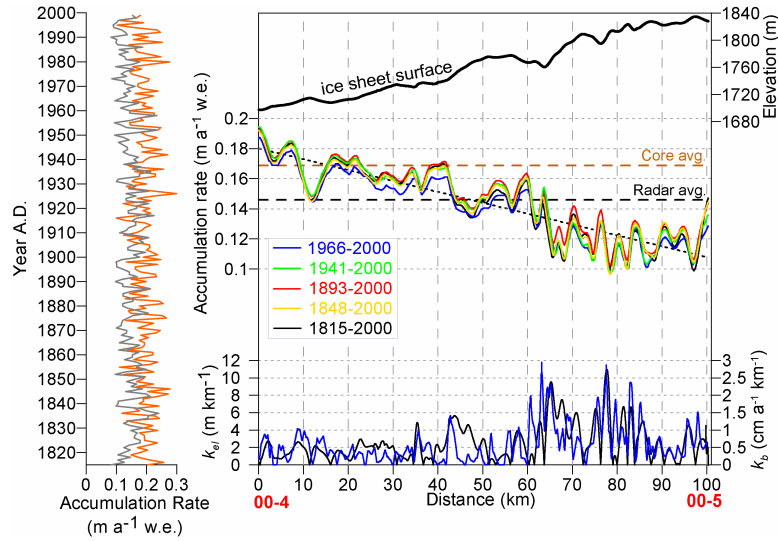


Figure 3: Spatial variability in accumulation rates from ice cores and GPR profiling. *Left:*

Annual  $\bar{b}$  for 00-4 (orange) and 00-5 (gray). *Top right:* Surface topography.

*Center right:* Calculated  $\bar{b}_r$  for each digitized horizon shown in Figure 2 (see legend). The sloping black line (short dashes) is the linear fit through the long-term  $\bar{b}_r$  based on the 1815 horizon. The core- (dashed orange line) and radar-

derived (dashed black line) means are also shown. *Bottom right:* Gradients along the elevation profile (black line) (*top right*) and the 1966-2000 accumulation rate profile (blue line) (*center right*).

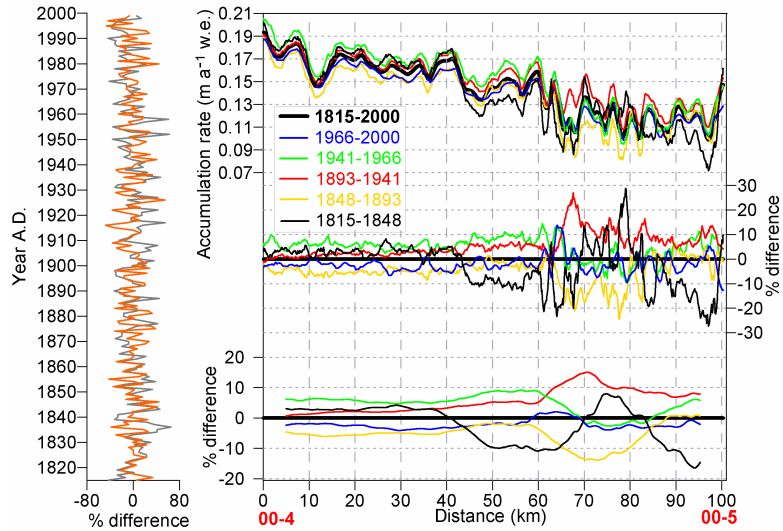


Figure 4: Temporal variability in accumulation rates from ice cores and GPR profiling.

*Left:* Percent difference from the core-derived average  $\bar{b}$  for 00-4 (orange) and 00-5 (gray). *Top right:* Calculated  $\bar{b}_r$  for each interval (see legend). The thick black line represents the long-term  $\bar{b}_r$  (1815-2000). *Center right:* Percent difference from the long-term  $\bar{b}_r$  for each horizon (see legend). *Bottom right:* Accumulation rate profiles (*center right*) after being smoothed. The 10-km smoothing clips the ends from each profile (see legend).